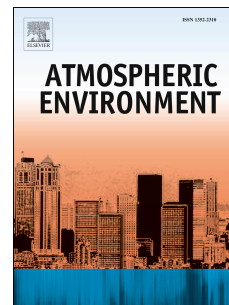# Accepted Manuscript

Seasonal light absorption properties of water-soluble brown carbon in atmospheric fine particles in Nanjing, China

Yanfang Chen, Xinlei Ge, Hui Chen, Xinchun Xie, Yuntao Chen, Junfeng Wang, Zhaolian Ye, Mengying Bao, Yanlin Zhang, Mindong Chen

Please cite this article as: Chen, Y., Ge, X., Chen, H., Xie, X., Chen, Y., Wang, J., Ye, Z., Bao, M., Zhang, Y., Chen, M., Seasonal light absorption properties of water-soluble brown carbon in atmospheric fine particles in Nanjing, China, *Atmospheric Environment* (2018), doi: 10.1016/j.atmosenv.2018.06.002.

Biomass burning
(Especially summer)

Seasonal variations

PM$_{2.5}$

Water extracts

Brown Carbon

ON Chromophores

Secondary reactions

Source areas
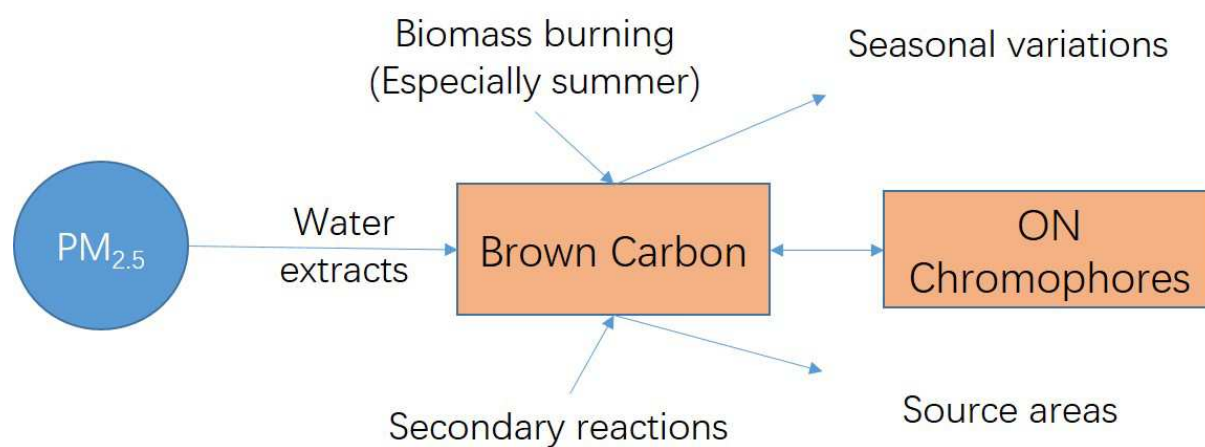
1   Seasonal light absorption properties of water-soluble brown carbon

2   in atmospheric fine particles in Nanjing, China

3   Yanfang Chen[a], Xinlei Ge[a*], Hui Chen[a], Xinchun Xie[a], Yuntao Chen[a],

4   Junfeng Wang[a], Zhaolian Ye[b], Mengying Bao[c], Yanlin Zhang[c], Mindong Chen[a]

5

6   [a]Jiangsu Key Laboratory of Atmospheric Environment Monitoring and Pollution

7   Control (AEMPC), Collaborative Innovation Center of Atmospheric Environment and

8   Equipment Technology (CIC-AEET), School of Environmental Science and

9   Engineering, Nanjing University of Information Science and Technology, Nanjing

10   210044, China

11   [b]College of Chemistry and Environmental Engineering, Jiangsu University of

12   Technology, Changzhou 213001, China

13   [c]Yale-NUIST Center on Atmospheric Environment, Nanjing University of

14   Information Science and Technology, Nanjing 210044, China

15

16   *Corresponding author, Email: caxinra@163.com

17   Phone: +86-25-58731394

18   For *Atmos. Environ.*

19

Abstract Recently atmospheric brown carbon (BrC) is recognized as an important contributor to light absorption and positive climate forcing. In this work, daily fine particulate matter ($PM_{2.5}$) samples were collected over a full year (May 2015 – May 2016) in Nanjing, and seasonal light absorptive properties of water-soluble BrC were investigated. We found that winter samples had the strongest light absorption among four seasons. The light absorption at 365 nm (Abs_{365}) for all seasons linked closely with secondary organic carbon (SOC), indicating a dominant contribution from secondary sources to BrC. However primary biomass burning might also contribute to BrC as revealed by the good correlations of Abs_{365} versus levoglucosan fragments and/or K^+, and such influence was more evident during summer. Furthermore, an Aerodyne soot-particle aerosol mass spectrometer (SP-AMS) was employed to determine the elemental ratios of BrC. We found that except in winter, the Abs_{365} in general positively correlated with the average oxidation states (OS_c) of BrC, suggesting more BrC were produced at higher OS_c. The mass absorption efficiency at 365 nm (MAE_{365}) showed no clear dependences on OSc during spring, summer and fall, but decreased against OS_c during winter, indicating chemical aging may lead to photo-bleaching of WSOM in winter. Moreover, positive responses of Abs_{365} to N/C ratios were found during all seasons, indicating nitrogen-containing organics can be important BrC chromophores. Potential source areas of BrC were further discussed to improve our understanding of BrC sources in this region. **Keywords:** Brown carbon; Light absorption; Aerosol mass spectrometry; Secondary aerosol; Biomass burning

1. Introduction

Atmospheric aerosol particles play an important role in earth's radiation budget and global climate change (e.g., Carslaw et al., 2010). Black carbon (BC) is typically treated as the most important aerosol component leading to positive radiative forcing (e.g., Bond et al., 2013; Wang et al., 2017). While recent studies indicate that a certain fraction of organic aerosols, often called "Brown carbon (BrC)" can also absorb lights at the wavelengths of near-ultraviolet (UV) and visible ranges (e.g., Bahadur et al., 2012; Cappa et al., 2012; Chen and Bond, 2010; Kirchstetter et al., 2004; Lack et al., 2012a; Laskin et al., 2015; Pokhrel et al., 2017; Saleh et al., 2013; Saleh et al., 2014). The radiative forcing of BrC has been estimated to be 19~24% of the total aerosol absorption (Feng et al., 2013; Liu et al., 2015; Zhang et al., 2017a).

Both laboratory and field studies have shown that BrC can be produced from multiple sources, including primary emissions from fossil fuel combustion (Bond et al., 2002; Yan et al., 2017) and biomass burning (Chakrabarty et al., 2010; Lack et al., 2012a; Washenfelder et al., 2015), as well as secondary formation through various reaction pathways including gas-phase and aqueous reactions (e.g., Hems and Abbatt, 2018; Laskin et al., 2015; Lin et al., 2015; Saleh et al., 2013; Zhong and Jang, 2011). The absorptivities of BrC generated from different sources are highly variable due to the different structures and concentrations of BrC chromophores (Laskin et al., 2015; Nguyen et al., 2012; Xie et al., 2017). A number of studies have been conducted to identify the BrC chromophores, but only a small fraction of organic chromophores

3

62 has been identified, including nitrophenols, aromatic carbonyls,

63 oxygenated–conjugated compounds, nitroaromatics and sulfur-containing compounds

64 (e.g., Desyaterik et al., 2013; Lin et al., 2015; Teich et al., 2017; Xie et al., 2017).

65 The BrC absorption can be directly measured by filter-based online instruments

66 (Kirillova et al., 2016; Nakayama et al., 2015), such as the multi-angle absorption

67 photometer (MAAP) and non-filter-based instruments (Laskin et al., 2015; Shamjad et

68 al., 2015), such as photoacoustic spectroscopy (PAS) and cavity ring-down (CRD)

69 spectroscopy (Lack et al., 2012a; Lack et al., 2006; Lack et al., 2012b; Pokhrel et al.,

70 2017; Pokhrel et al., 2016). Moreover, water-soluble BrC has been measured

71 semi-continuously by a particle-into-liquid sampler (PILS), coupled to a liquid

72 waveguide capillary cell (LWCC) and an absorbance spectrometer (Liu et al., 2013;

73 Satish et al., 2017). In addition, light absorption measurements on offline filter

74 extracts have been conducted in both laboratory (e.g., Chen and Bond, 2010; Liu et al.,

75 2016) and field studies (e.g., Chen et al., 2016; Zhang et al., 2017c). The advantage of

76 this approach is that the interference by BC can be avoided. Compared to the online

77 methods, offline technique can be easily performed in combination with other offline

78 measurements for a better characterization of BrC.

79 The Yangtze River Delta (YRD) region is one of the most populated areas in

80 China. Nanjing, as the second largest city and the provincial capital of Jiangsu

81 Province, is also facing severe air pollution issue (Wang et al., 2016a). Some studies

82 (e.g., Wu et al., 2017; Zhang et al., 2017b; Zhang et al., 2015) show that the organic

83   aerosols (OA) can account for a remarkable proportion of fine aerosol mass and are

84   originated from multiple sources, including primary (traffic, cooking, industry,

85   biomass burning and biogenic emissions) and secondary sources (aqueous-phase and

86   photochemical processing). Hundreds of organic species (polycyclic aromatic

87   hydrocarbons, carboxylic/dicarboxylic acids, hopanes, phthalates, amines and amino

88   acids, etc.) have been identified (e.g., Wang et al., 2011; Wang et al., 2009; Wang et

89   al., 2007). Recently, a 3-year result of light absorption of BrC in Nanjing based on

90   continuous measurement combined with Mie-theory calculations was reported (Wang

91   et al., 2018). The results demonstrate a significant contribution of BrC to total aerosol

92   absorption (from 6% to 18%, and up to ~28% in biomass burning dominant season

93   and winter). Nevertheless, studies regarding the light absorption of BrC are still scarce

94   in this region. In this work, we investigated the light absorption properties of the

95   water-soluble BrC via a series of offline measurements for $PM_{2.5}$ samples collected in

96   Nanjing during 2015~2016. We focus on its seasonal behaviors, sources and

97   dependences on bulk chemical properties.

98

99   **2. Experimental Methods**

100   *2.1 Sample collection*

101   A high-volume sampler (Laoying Ltd., Qingdao, model 2031) with a flow rate of

102   1.05 $m^3 min^{-1}$ was set on rooftop of a seven-floor building (~21 m above the ground)

103   inside the campus of Nanjing University of Information Science and Technology in

104   the northern suburb of Nanjing (32.21°N, 118.72°E) (Figure S1 in the supplement).

105   More details can be found in our previous study (Wang et al., 2016b). A total of 272

106   $PM_{2.5}$ samples were collected daily (22 hours, from 12:00 p.m. to 10:00 a.m. of the

107   next day) from May 4, 2015 to 4 May, 2016. The samples were collected onto

108   pre-baked (450 ^{o}C for 4 hours) quartz fiber filters (8×10 inch, Pall Life Science, USA).

109   Two field blanks were treated in the same manner as for the samples. The $PM_{2.5}$ mass

110   concentrations were determined gravimetrically using a digital balance (OHAUS

111   DV215CD, precision 0.01 mg) immediately after filter collection. The filters were

112   then wrapped in aluminum foil, sealed in polyethylene bags and stored at -18 ^{o}C until

113   analysis.

114   During sampling, meteorological parameters (temperature, relative humidity,

115   wind speed, wind direction) were recorded at the meteorological station located near

116   the sampling site (~50m distance). Original hourly data were averaged into daily data.

117

118   *2.2 Chemical analyses*

119   **OC/EC:** One punched piece (diameter: 17 mm) of each filter was analyzed for

120   organic carbon (OC) and elemental carbon (EC) contents by the thermal-optical

121   OC/EC analyzer (Sunset Laboratory, USA) following the standard protocol (Birch

122   and Cary, 1996; Cao et al., 2017).

123   **Ionic species:** Two 10 mm diameter filter punches of each filter were extracted

124   with 15 mL ultrapure water (18.2MΩ cm, TOC< 5ppb), sonicated for 40 min at 0 ^{o}C in

125 an ice-water bath, filtrated through 0.45 μm syringe filters (Spartan, Whatman). K^+

126 concentrations used in this work were determined by an ion chromatograph (Aquion,

127 Thermo Fisher Scientific, Waltham, MA, USA) equipped with a Dionex CS12A

128 column (20mM methanesulfonic acid as eluent). Instrument and operational details

129 are the same as those described in Ye et al. (2017b).

130 **WSOC and UV-Vis absorption**: A quarter of each filter was extracted with 100

131 mL ultrapure water similar as for ionic species. The water-soluble OC (WSOC)

132 concentrations were quantified by a TOC-VCPH analyzer (Shimazu, Japan) using a

133 thermo-catalytic oxidation approach. Detailed procedures are described in Ge et al.

134 (2014). The ultraviolet-visible (UV-Vis) light absorption spectra of the water extracts

135 were measured using a UV-Vis spectrophotometer (UV-3600, Shimadzu, Japan) as

136 described in Zhang et al. (2013).

137 **WSOM:** The offline SP-AMS analysis details were similar to those reported

138 previously (e.g., Ye et al., 2017a; Ye et al., 2017c). Briefly, the water extracts were

139 nebulized with argon using a constant output atomizer (TSI Model 3076). The

140 generated aerosols were dehumidified by a silica gel diffusion dryer, and subsequently

141 analyzed by the SP-AMS. Purified water was aerosolized before every sample

142 measurement to cleanse the system, and extracts of blank filters were treated in the

143 same way as a system blank. Note the offline AMS technqiue was mainly used to

144 obtain the ion-speciated mass spectra of water-soluble organic matter (WSOM) (e.g.,

145 Chen et al., 2017; Daellenbach et al., 2016; Daellenbach et al., 2017; Ge et al., 2017;

146   Ye et al., 2017a). In this work, we only used the elemental ratios determined by the

147   SP-AMS measurements. Examples of the high resolution mass spectra(HRMS) of

148   WSOM were presented in Fig. S2. Detailed mass spectral analyses and source

149   apportionment of WSOM will be presented in our future work.

150

151   *2.3 Data analyses*

152   *2.3.1 Light absorption coefficients*

153   The UV-Vis light absorption data were fitted into a power law function

154   (Hecobian et al., 2010) over the range 300~600 nm according to:

155     $$\text{Abs}_\lambda = k \cdot \lambda^{-Å} \tag{1}$$

156   Where Abs_λ is the light absorbance at wavelength λ, k is a scaling constant, and Å is

157   the absorption Ångström exponent (AAE) which describes the spectral dependence of

158   light absorption from chromophores in solution.

159   The light absorption data is converted to an absorption coefficient at a

160   wavelength λ (Abs_λ, Mm^{-1}) by equation (2) (Hecobian et al., 2010):

161     $$\text{Abs}_\lambda = (A_\lambda - A_{700}) \cdot \lambda \frac{V_l}{V_a \cdot L} \ln(10) \tag{2}$$

162   Where A_{700} (mean value of 695 - 705 nm) is a reference to account for baseline drift,

163   V_l is the volume of water that filter was extracted into, V_a is the volume of sampled air,

164   and L is the optical path length (1 cm) of the quartz cuvette in the UV-vis

165   spectrometer.

166   The mass absorption efficiency (MAE, $m^2 g^{-1}$) at 365 nm was then calculated by

167   equation (3): $MAE_{365} = \frac{Abs_{365}}{C_{WSOC}}$ (3)

168   Where C_{WSOC} is the WSOC concentration. We used WSOC concentrations here for

169   consistency and comparison with previous results. In fact, as we are able to calculate

170   the WSOM concentrations (Section 2.3.2), we can determine MAE_{365} using

171   Abs_{365}/C_{WSOM}. Scatter plot of the two sets of MAE_{365} was shown in Fig. S3. They

172   correlated very well (r of 0.96) but differed with a factor of ~2 as the average OM/OC

173   ratio was ~2 (Section 2.3.2).

174   *2.3.2 Elemental and OM/OC ratios of WSOM*

175   The SP-AMS data were analyzed using the Igor-based ToF-AMS Analysis

176   Toolkit (Squirrel v.1.57A and Pika v1.16A, available at:

177   http://cires.colorado.edu/jimenez-group/ToFAMSResources/ToFSoftware/). The CO^+

178   signals were from fragmentation of organic species without influences from N_2^+

179   signals, as we used argon as carrier gas. Due to the possible influences from

180   carbonates on organic CO_2^+ signals (Bozzetti et al., 2017; Xu et al., 2013), we set it

181   equal to CO^+. Signals of H_2O^+, HO^+ and O^+ were then scaled to CO_2^+ according to

182   Aiken et al. (2008)): $H_2O^+ = 0.225 \times CO_2^+$, $HO^+ = 0.05625 \times CO_2^+$, and

183     $O^+ = 0.009 \times CO_2^+$.

184   The oxygen-to-carbon (O/C) and hydrogen-to-carbon (H/C) ratios were

185   calculated according to Canagaratna et al. (2015), nitrogen-to-carbon (N/C) ratios

186   were derived based on Aiken et al. (2008), all of which were used to calculate the

187   organic matter-to-organic carbon (OM/OC) ratios. The WSOM concentrations were

9

188 then calculated by using the WSOC concentrations determined by the TOC analyzer

189 (Section 2.2) and the OM/OC ratios (OM/OC$_{WSOM}$), as shown in equation (4):

190
$$WSOM = WSOC \cdot (OM/OC)_{WSOM} \tag{4}$$

191 The annual average OM/OC ratio was 2.02 ± 0.1 (average $\pm 1 \sigma$)(1.79~2.24),

192 consistent with the values for WSOM reported earlier (Xu et al., 2017; Ye et al.,

193 2017c).

194 *2.3.3 Primary and secondary OC estimations*

195 The EC-tracer method (Turpin and Huntzicker, 1995) was used to infer the

196 primary OC (POC) and secondary OC (SOC), as follows:

197
$$POC = EC \cdot (OC/EC)_{pri} \tag{5}$$

198
$$SOC = OC - POC \tag{6}$$

199 Where (OC/EC) $_{pri}$ refers to the OC/EC ratio for primary OA, and the minimum

200 measured value (1.63) among all samples was used here. It should be noted that such

201 treatment may introduce uncertainties as the primary OA (such as biomass burning

202 and coal combustion emissions) may have large OC/EC ratios, and the ratios also vary

203 among different sources. However, as EC is exclusively from primary sources, the

204 POC scaled from EC also come from primary sources; the accuracy of POC/SOC

205 estimates is difficult to quantify, a reasonable estimate is <20% for our study based on

206 Wu and Yu (2016), considering the measurement uncertainties of <12% for OC and

207 EC (Ye et al., 2017c), an average SOC/OC of 0.65, and a sampling size of 272.

208 In addition, the concentrations of water-insoluble organic carbon (WIOC) can be

10

209   calculated by equation (7):

210                                    $WIOC = OC - WSOC$ (7)

211   *2.3.4 Air mass trajectories*

212   The calculations were carried out with ZeFir, an Igor-based tool (Petit et al.,

213   2017). The 36-h back trajectories (at 500m height) were calculated by the HYbrid

214   Single-Particle Lagrangian Integrated Trajectory (HYSPLIT, version 4.8) model

215   (Stein et al., 2016) developed by the National Oceanic and Atmospheric

216   Administration Air Resources Laboratory.

217   *2.3.5 Potential source contribution analyses*

218   The potential source contribution function (PSCF) analysis was performed to

219   explore the air mass origins and to identify potential source areas. The methodology is

220   described elsewhere (Polissar et al., 1999). Briefly, the PSCF is calculated as:

221                                    $PSCF_{ij} = \dfrac{m_{ij}}{n_{ij}}$ (8)

222   Where n_{ij} is the total number of trajectory endpoints in the ij^{th} cell, and m_{ij} is the

223   number of trajectory endpoints in the ij^{th} cell associated with values above the

224   threshold value. The PSCF analysis was also carried out with the ZeFir toolkit with a

225   resolution of 0.2º×0.2º for each grid cell. The 75th percentile was chosen as the

226   threshold value to calculate m_{ij}. In order to reduce the influences of small n_{ij} on the

227   PSCF values, a weighing function has been implemented (Petit et al., 2017):

228
$$w_{ij} = \begin{cases} 1.00 & \text{for } n_{ij} \geq 0.85 \max(\log(n_{ij} + 1)) \\ 0.725 & \text{for } 0.6 \max(\log(n_{ij} + 1)) < \log(n + 1) \\ & \leq 0.85 \max(\log(n_{ij} + 1)) \\ 0.475 & \text{for } 0.35 \max(\log(n_{ij} + 1)) < \log(n + 1) \\ & \leq 0.6 \max(\log(n_{ij} + 1)) \\ 0.175 & \text{for } \log(n + 1) \leq 0.35 \max(\log(n_{ij} + 1)) \end{cases} \quad (9)$$

229

230 **3. Results and discussion**

231 *3.1 Wavelength dependence of light absorption*

232   The samples were classified into spring (March-May, *n*=85), summer

233 (June-August, *n*=45), fall (September-November, *n*=64) and winter

234 (December-February, *n*=78). Figure 1a presents the average light absorption spectra of

235 the water-soluble species during four seasons and the full year within the wavelength

236 (λ) range of 300 -600 nm. Overall, the average light absorption of winter samples was

237 significantly higher than those of spring, summer and fall, and leading to a relatively

238 high annual absorption spectrum. This is corresponding to the high concentrations of

239 light-absorbing species in winter samples (details in Section 3.2). The absorption

240 intensities for all samples increased sharply towards shorter wavelengths. Such shapes

241 are consistent with previous findings of BrC (e.g., Chen et al., 2016; Hecobian et al.,

242 2010; Liu et al., 2013), indicating that the WSOM (or a fraction of WSOM) obtained

243 in this study was BrC.

244   We further calculated the AAE values through the linear regression of log(Abs)

245 *vs.* log(λ) (the natural logarithmic form of equation (1)) in the wavelength range of

12

246   300~600 nm. The AAE values and relevant optical properties of BC and BrC can

247   differ substantially among different situations. Several studies report that the AAE of

248   fresh BC particles is ~ 1 (e.g., Bond, 2001; Kirchstetter et al., 2004), while the BC

249   particles with thicker coating can have a higher AAE (as large as 1.6) even the coating

250   species do not absorb light (Gyawali et al., 2009). Gyawali et al. (2009) also

251   illustrates that vehicular-related and biomass burning aerosols have different optical

252   characteristics. Much higher AAE values ranging from ~3 to ~12 are reported for

253   water extracts of ambient aerosols collected from urban and rural sites (Cheng et al.,

254   2016; Du et al., 2014; Kim et al., 2016; Kirillova et al., 2014; Yan et al., 2015; Zhu et

255   al., 2017). The laboratory chamber generated particles from various wood smoldering

256   can also have large AAE values between ~7 and ~16 (Chen and Bond, 2010). It is also

257   worth to mention that AAE is also pH-dependent (Mo et al., 2017; Phillips et al.,

258   2017).

259   In this work, the average AAE values during four seasons were 7.15, 7.28, 6.84

260   and 6.74, respectively (Fig. 1b). The annual average AAE value was 6.89. Different

261   from the absorption spectra shown in Fig. 1a, the AAE value during winter was the

262   lowest while the mean AAE of summer samples was the largest, suggesting

263   remarkably different chemical compositions and/or sources of BrC during four

264   seasons. Overall, the level of AAE values observed here is comparable with some

265   previous results determined for the water-soluble $PM_{2.5}$ species extracted by using the

266   similar extraction protocols, such as in Tibetan Plateau (6.2 and 6.9) (Zhang et al.,

13

267 2017c; Zhu et al., 2017), Beijing, China（7.2 ~ 7.5) (Cheng et al., 2011), and Los

268 Angeles basin (7.6) (Zhang et al., 2013), etc. But the AAE values also appear to be

269 higher than those in high-altitude Himalayas areas (3.9~5.6) (Kirillova et al., 2016),

270 Seoul, Korea (5.84 in winter) (Kim et al., 2016), These studies demonstrate that the

271 BrC might be related to primary biomass burning emissions and/or photochemical

272 SOA formed from anthropogenic gaseous precursors, which are implicate for the BrC

273 source analyses in Nanjing as well.

274

275 *3.2 Seasonal variations and sources*

276   We calculated the light absorption at 365 nm (Abs_{365}, in M m^{-1}) as a proxy to

277 represent the light absorption of water-soluble BrC, as Abs_{365} can avoid interferences

278 from non-organic species (such as inorganic nitrate) (Hecobian et al., 2010). The time

279 series of Abs_{365}, MAE_{365}, RH, temperature, wind direction (colored by wind speed),

280 and the concentrations of $PM_{2.5}$, WSOC, OC, EC and K^+, over the full year are

281 displayed in Fig. 2. Correspondingly, the seasonal and annual averaged values of the

282 aerosol species, Abs_{365} and MAE_{365} are further shown in Fig. 3a. The annual average

283 $PM_{2.5}$, OC, WSOC, EC, K^+, Abs_{365} and MAE_{365} values were 114.5 µg m^{-3}, 15.2 µg

284 m^{-3}, 7.2 µg m^{-3}, 3.2 µg m^{-3}, 0.7 µg m^{-3}, 5.7 M m^{-1} and 0.76 m^2 g^{-1} C, respectively. In

285 particular, the annual MAE_{365} value is much lower than the results determined by a

286 multi-wavelength Aethalometer (Model AE-31) in Xianghe, China (2.2 at 370 nm)

287 (Yang et al., 2009) and Nanjing (11.4 in winter and 8.6 in summer) (Wang et al.,

14

288 2018), methanol-extracted BrC in Beijing (1.45) (Cheng et al., 2016), in Los Angeles

289 basin (2.27) (Zhang et al., 2013). But the value is also comparable with some previous

290 values determined by online PILS-LWCC-TOC system (0.71) (Zhang et al., 2013),

291 and those in Southeastern United States (0.64 in 8 urban sites and 0.58 in 6 rural sites)

292 (Hecobian et al., 2010) and Central Indo Gangetic Plain (1.16) (Satish et al., 2017),

293 etc.

294   The annual WSOC/OC ratio was 0.46 ± 0.1, highest in summer (0.59 ± 0.12),

295 followed by fall (0.49 ± 0.09), winter (0.47 ± 0.08) and spring (0.43 ± 0.12). These

296 ratios are well within the range of WSOC/OC ratios reported earlier (Ye et al., 2017b;

297 Zhang et al., 2018). The SOC/POC ratios were 2.11 ± 1.28, 1.83 ± 1.19, 2.28 ± 1.28

298 and 3.17 ± 1.66 in spring, summer, fall and winter, respectively. The Abs_{365} value was

299 highest during winter (9.44 ± 4.70 M m^{-1}) and lowest during summer (3.31 ± 2.36 M

300 m^{-1}), while the spring and fall samples had similar values of 4.32 ± 2.28 and $4.70 \pm$

301 2.35 Mm^{-1}, respectively. The seasonal order of Abs_{365} values was in line with their

302 corresponding $PM_{2.5}$/OC/WSOC concentrations, indicating the close relationships

303 between the BrC light-absorbing ability with levels of aerosol pollutions. The

304 seasonal variability also reflected the differences of concentrations of BrC species,

305 sources and water solubility of the light-absorbing chromophores. A similar seasonal

306 trend of Abs_{365} is also reported in Seoul, Korea (Kim et al., 2016), but its value

307 ($0.87 \sim 7.31$ M m^{-1}) is lower than those determined here. The Abs_{365} seasonal behavior

308 (lowest Abs_{365} in summer and highest in winter) is also similar with those observed in

309   other areas of China. For examples, the Abs_{365} values in Beijing, China (Du et al.,

310   2014) are 4.6 M m^{-1} in spring, 3.7 M m^{-1} in summer, 9.1 M m^{-1} in fall and 10.1 M m^{-1}

311   in winter; in another study, the Abs_{365} values over the southeastern Tibetan Plateau

312   (Zhu et al., 2017) are 0.85 M m^{-1} in spring, 0.38 M m^{-1} in summer, 0.55 M m^{-1} in fall

313   and 1.04 M m^{-1} in winter. Moreover, the MAE_{365} of the four seasons were 0.69 m^2 g^{-1}

314   C, 0.51 m^2 g^{-1} C, 0.70 m^2 g^{-1} C and 1.04 m^2 g^{-1} C during spring, summer, fall and

315   winter, respectively, which was also in the same order as that of Abs_{365} (Fig. 3a). This

316   result highlights that for the same amount of BrC, those during winter appear to have

317   a stronger light-absorbing ability.

318   Figure 3b shows the correlation coefficients (r) of Abs_{365} versus $PM_{2.5}$, OC,

319   WSOC, EC and K$^+$ for different seasons and the whole year. Generally, the

320   correlations with WSOC were strong across four seasons (r of 0.80~0.93), and on a

321   yearly basis, the correlation coefficient was 0.85 (Fig. 4a). Together, these results

322   suggest that a significant fraction of WSOC is BrC chromophores and the similar

323   sources for WSOC and water-soluble BrC throughout the year. The correlations

324   between Abs_{365} and OC were also tight (r of 0.82~0.93) as the temporal variations of

325   OC varied closely with WSOC in this study (r of 0.91, Fig. 4b). The correlation of

326   Abs_{365} versus EC was weak, ranging from 0.33 to 0.51 for the four seasons (r of 0.36

327   for all samples). Similarly, the correlation coefficient between Abs_{365} and POC was

328   also 0.36 (Fig. 4c) as the POC concentrations were directly scaled from EC using

329   equation (5) in this study. On the contrary, the correlation between Abs_{365} with SOC

330   was apparently much tighter (r of 0.86, Fig. 4e). These results demonstrate that the

331   water-soluble BrC is abundant of secondarily formed species rather than the primary

332   species. Correspondingly, it is expected that the SOC was strongly associated with

333   WSOC (r of 0.89, Fig. 4f), while the POC was more likely composed of WIOC (r of

334   0.61, Fig. 4d). The weak correlation of water-soluble BrC Abs_{365} with POC was likely

335   due to the low-water solubility of primary organic species, while the water-soluble

336   BrC Abs_{365} correlated moderately with WIOC (r of 0.78, Fig. S4), likely indicating

337   similar sources for WSOC and WIOC. Nevertheless, the light absorption properties of

338   water-insoluble aerosol species remain to be elucidated.

339   In addition, K^+ ion is often used as a primary biomass burning emission tracer

340   (Chow et al., 2007). Concentrations of this ion correlated much better with Abs_{365}

341   during summer (r of 0.87, Fig. 3b) than those during spring (r of 0.56), fall (r of 0.46)

342   and winter (r of 0.51). This finding suggests that besides secondary sources, biomass

343   burning can also contribute to the BrC evidently in summer. This is consistent with a

344   recent study (Wang et al., 2018), which also suggests that biomass burning was an

345   important source of BrC during summer in Nanjing. Cheng et al. (2013) also shows

346   that K^+ as a biomass burning tracer is reliable during summer.

347   As is well known, levoglucosan ($C_6H_{10}O_5$) is another common biomass burning

348   tracer compound (Simoneit, 2002; Simoneit et al., 1999). Correspondingly, $C_2H_4O_2^+$

349   and $C_3H_5O_2^+$ ions are electron impact ionization fragments of levoglucosan and they

350   are often used as biomass burning OA marker ions in the AMS spectral analyses

17

351 (Alfarra et al., 2007; Ge et al., 2012). Therefore, we investigated the correlations

352 between BrC Abs_{365} with these two AMS ions. Their concentrations were calculated

353 based on their corresponding mass fractional contributions in the WSOM AMS

354 spectra and the WSOM mass concentrations derived from equation (4). As shown in

355 Fig. 5, the BrC Abs_{365} overall showed good correlations with both $C_2H_4O_2^+$ (r of

356 0.83~0.97) and $C_3H_5O_2^+$ (r of 0.73~0.95). Somewhat different from the correlations

357 with K^+, this result indicates the possible influences of biomass burning on the BrC

358 light absorption throughout the year. But still, summer samples correlated the best

359 with $C_2H_4O_2^+$ (r of 0.97) and $C_3H_5O_2^+$ (r of 0.95) among four seasons, again

360 suggesting a more obvious influence during summer than during other seasons from

361 biomass burning. Note the good correlations with biomass burning tracer species

362 indicate that biomass burning can contribute to the BrC, but does not mean it is the

363 dominant contributor.

364

365 *3.3 Influences of bulk chemical properties*

366 To further unravel the features of water-soluble BrC in Nanjing, we examined the

367 dependence of seasonal behaviors of Abs_{365} on the bulk properties of WSOM. We first

368 plotted the Abs_{365} as a function of the average oxidation states (OS_c, defined as

369 $2\times O/C-H/C$) (Kroll et al., 2011) of WSOM for different seasons in Figs. 6a-d.

370 Although there are large uncertainties, statistically the Abs_{365} values presented an

371 increasing trend with OS_c for spring, summer and fall samples, while there was no

372 clear positive correlation between Abs_{365} and OS_c for winter samples. Similar features

373 were observed for Abs_{365} versus O/C ratios too in Fig. S5. Consistently, the light

374 absorption (Abs_{365}) tended to decrease with the increase of H/C during spring,

375 summer and fall, but the trend was less clear-cut during winter as well (Fig. S6).

376 These plots suggest that more BrC were produced at higher OS_c. It should be noted

377 that, previous studies report that the optical properties of atmospheric BrC species can

378 be altered significantly during atmospheric ageing, but the ageing processes may lead

379 to photo-enhancement (Bones et al., 2010; Updyke et al., 2012) or photo-bleaching

380 (Lee et al., 2014; Liu et al., 2016; Sumlin et al., 2017; Zhao et al., 2015), dependent

381 upon the types of precursors and reaction conditions. As OS_c is a metric of the ageing

382 extent, the unique behavior of winter samples likely reflects that the dominant ageing

383 processes or the precursors to form BrC in winter are different from those in other

384 seasons in Nanjing. Of course, OS_c merely represents the average properties of BrC,

385 future molecular characterization of BrC would be essential to under the ageing

386 processes and their impacts on BrC light absorption in details. In addition, the Abs_{365}

387 correlated very well with SOC (Fig. 4e) while the correlation with OSc was not so

388 tight. This is because OS_c was for WSOA while SOC was for bulk OC, and SOC itself

389 may not perfectly with OSc as well, due to that SOC is an assemble of species from

390 multiple oxidation processes and precursors.

391   To further investigate the BrC absorption efficiencies, we plotted MAE_{365} against

392 OSc in Figs. 6e-h. Generally, we observed no positive dependences of MAE_{365} on OS_c

393   during spring, summer and fall, indicating that the "absorption efficiency" of WSOM

394   did not change obviously with chemical aging during the three seasons. On the other

395   hand, the MAE_{365} of winter WSOM presented a decreasing trend with OS_c, showing

396   that aging may lead to photo-bleaching of WSOM in winter.

397   As recent studies (e.g., Budisulistiorini et al., 2017) report that nitrogen (N)- or

398   sulfur-containing organic compounds are possible BrC chromophores. Here, we

399   investigated Abs_{365} as well as MAE_{365} against N/C ratios during four seasons in Fig. 7

400   (we did not calculate Abs_{365} versus S/C ratios, as S/C ratios were very small and noisy

401   in this work). Except a few outliers in summer and fall, generally speaking, both

402   Abs_{365} and MAE_{365} values seemed to positively respond to the increase of N/C ratios

403   during all time. This result manifests that N-containing organics are effective BrC

404   light-absorbing chromophores in Nanjing. Nitroaromatic compounds were identified

405   as important BrC compounds previously in biomass burning emissions (Cao et al.,

406   2017; Lin et al., 2016). Note we indeed observed N-containing ion fragments with a

407   benzene ring in the AMS spectra, suggesting the existence of nitroaromatics in our

408    $PM_{2.5}$ samples even though in a very low level. Therefore, results in Fig. 7 likely

409   verifies the possible contribution of biomass burning to BrC as well. Of course, a

410   majority of the N-containing organic fragments in the AMS spectra are small *m/z* ions

411   without a benzene ring, which are likely from other types of organic nitrogen species,

412   including amines, amino acids, amides etc (Ge et al., 2011a, b). Whether or not these

413   species are effective chromophores, their sources, formations and contributions to

20

414   light absorption, are yet to be carefully investigated in the future.

415

416   *3.4 Potential source areas*

417   The potential source contributions (PSC) from different geological locations to

418   the water-soluble BrC Abs_{365} were illustrated in Fig. 8. We also conducted the back

419   trajectory analyses and presented the results in Figs. 9 and 10 for the four seasons.

420   Winter air masses can be classified into four clusters while three clusters were

421   identified for other seasons. There were significantly different source area

422   contributions among four seasons to the Abs_{365}.

423   During spring, the BrC potential source areas mainly distributed in the southwest

424   and southeast of Nanjing, consistent with the cluster analyses of air mass back

425   trajectories shown in Fig. 9a. The average values of Abs_{365} from Cluster 1 and Cluster

426   2 were much higher than that of Cluster 3 (Fig. 10a). Cluster 1 (46.3% of total

427   trajectories) had a relatively short length, intercepting the local/regional emissions in

428   the Yangtze River Delta (YRD) region. Cluster 2 (38.1%) originated from Hunan

429   province and travelled across Anhui province, which could also play an important role

430   in affecting the absorbability of BrC in Nanjing in spring. Cluster 3 (15.6%) started

431   from Liaoning province, and passed through Bohai Sea, Shandong Peninsula and

432   Huanghai Sea, which delivered relatively clean air, and had less influences on BrC. In

433   addition, the PSC distributions of Abs_{365} were also similar to those of SOC (Fig. S7a)

434   but not to POC (Fig. S8a) and K^+ (Fig. S9a), supporting that secondary source was a

21

435   dominant contributor of BrC during spring.

436   During summer, the BrC potential source areas mainly located in southeast of

437   Nanjing (<100 km), confined within a relatively small region in Jiangsu and Anhui

438   Provinces (Fig. 8b). Correspondingly, the air masses were also dominated by Cluster

439   1 (60%) with very short length (Fig. 9b). It should be noted that, the PSC hotspots of

440   SOC (Fig. S7b), POC (Fig. S8b) and K^+ (Fig. S9b) also appeared in the southeast near

441   Nanjing, indicating the important contributions from both primary (biomass burning)

442   and secondary sources. Cluster 3 (17.8%) passed through the North China Plain (NCP)

443   and the corresponding BrC seemed to be the most light-absorptive among the three

444   clusters. Cluster 2 (22.2%) originated from Huanghai Sea and bring about less BrC

445   compounds. In addition, maps of the fire spots in China during 2015 summer were

446   presented in Fig. S10a-c. Obviously, lots of fire points were found in the regions

447   overlapping with trajectories of Cluster 1 and Cluster 3, proving the biomass burning

448   influences on BrC during summer. Such burning activities along with these clusters

449   likely include crop burning during harvest seasons.

450   In fall, local Nanjing and Anhui Province were identified as the most potential

451   source areas, as shown in Fig. 8c. Correspondingly, the BrC in Cluster 3 from such

452   areas apparently had a higher light absorptivity than those in the other clusters (Fig.

453   10c), although it was not dominant (31.1%, less than 45.3% of cluster 2 from

454   Huanghai Sea) (Fig. 9c). Also, the Abs_{365} PSC distributions were highly similar to

455   SOC (Fig. S7c) rather than POC (Fig. S8c) and K^+ (Fig. S9c) indicating a more

22

456   significant role of secondary source to BrC during fall.

457   For the case of winter, the potential source areas mainly located close to the

458   sampling site (Fig. 8d). Correspondingly, the dominant air mass trajectory (Cluster 1,

459   52.56%) was also the shortest. Hotspots of SOC (Fig. S7d), POC (Fig. S8d) and K^+

460   (Fig. S9d) were all concentrated in a narrow region, all demonstrating that overall

461   local emissions might be major sources of these species and BrC. Such local

462   emissions may also include enhanced residential burning (such as cookstove

463   emissions) during winter. However, on average, the BrC with large light absorptivity

464   was not from Cluster 1, but from Cluster 2 (10.26%) and Cluster 4 (15.38%), which

465   passed through NCP and southern China, respectively (Fig. 10d). This was also likely

466   associated with BrC from biomass burning, and further inspection indeed found lots

467   of fire events in these regions during February (Fig. S10f). While during the other two

468   months, biomass burning unlikely played important roles but more likely

469   contributions from secondary and aged local emissions were important.

470

471   **4. Conclusions**

472   This work investigated the light absorption properties and sources of

473   water-soluble BrC in atmospheric fine particles collected from 4 May 2015 to 4 May

474   2016 in Nanjing. We also conducted chemical analyses of OC, EC, WSOC, K^+, and

475   SP-AMS analyses on the water-soluble organics. The light absorption and mass

476   absorption efficiency at 365 nm were found to be both stronger during winter than

477 during other seasons. The AAE values were in a range of 6.74~7.28 with an annual

478 average of 6.89. The BrC light absorption at 365 nm (Abs_{365}) correlated very well

479 with SOC during all seasons, indicating a significant contribution from secondary

480 sources. We also investigated the correlation between Abs_{365} and the biomass burning

481 marker K^+ and levoglucosan (using its AMS fragments), and found that t biomass

482 burning could contribute to BrC as well, but more evidently in summer.

483   The Abs_{365} generally positively responded to the increase of OS_c during spring,

484 summer and fall, indicating more BrC at higher OS_c. While the dependences of

485 MAE365 against OSc were less clear-cut during these three seasons, MAE365 during

486 winter displayed an decreasing trend against OSc , implying chemical aging may lead

487 to photo-bleaching of BrC in winter. Furthermore, overall positive correlations of

488 Abs_{365} and MAE_{365} with N/C ratios were found throughout the year, suggesting that

489 nitrogen-containing organics are important BrC chromophores in Nanjing. PSCF

490 analyses further showed the different source regions to BrC during different seasons,

491 and in particular, pointed out that biomass burning in North China Plain or sometimes

492 southern China could have more impacts on BrC during summer and winter

493 (especially February in this work). Overall, our study provides valuable insights into

494 BrC in densely populated regions. Future investigations are strongly needed,

495 including investigation of light absorption properties of water-insoluble species,

496 quantification of the contributions from primary and secondary sources to BrC, and

497 the molecular characterization of possible BrC chromophores, etc.

Acknowledgements

Appendix A. Supplementary data

Supplementary data related to this article can be found at: xxx….

References

Aiken, A.C., Decarlo, P.F., Kroll, J.H., Worsnop, D.R., Huffman, J.A., Docherty, K.S., Ulbrich, I.M., Mohr, C., Kimmel, J.R., Sueper, D., Sun, Y., Zhang, Q., Trimborn, A., Northway, M., Ziemann, P.J., Canagaratna, M.R., Onasch, T.B., Alfarra, M.R., Prevot, A.S.H., Dommen, J., Duplissy, J., Metzger, A., Baltensperger, U., Jimenez, J.L., 2008. O/C and OM/OC ratios of primary, secondary, and ambient organic aerosols with high-resolution time-of-flight aerosol mass spectrometry. Environ. Sci. Technol. 42, 4478-4485.

Alfarra, M.R., Prevot, A.S.H., Szidat, S., Sandradewi, J., Weimer, S., Lanz, V.A., Schreiber, D., Mohr, M., Baltensperger, U., 2007. Identification of the mass spectral signature of organic aerosols from wood burning emissions. Environ. Sci. Technol. 41, 5770-5777.

Bahadur, R., Praveen, P.S., Xu, Y., Ramanathan, V., 2012. Solar absorption by elemental and brown carbon determined from spectral observations. P. Natl. Aacd. Sci. USA 109, 17366-17371.

Birch, M.E., Cary, R.A., 1996. Elemental carbon-based method for monitoring occupational exposures to particulate diesel exhaust. Aerosol Sci. Technol. 25, 221-241.

Bond, T.C., 2001. Spectral dependence of visible light absorption by carbonaceous particles emitted from coal combustion. Geophys. Res. Lett. 28, 4075-4078.

Bond, T.C., Covert, D.S., Kramlich, J.C., Larson, T.V., Charlson, R.J., 2002. Primary particle emissions from residential coal burning: Optical properties and size distributions. J. Geophys. Res. - Atmos. 107, 8347.

Bond, T.C., Doherty, S.J., Fahey, D.W., Forster, P.M., Berntsen, T., DeAngelo, B.J., Flanner, M.G., Ghan, S., Kärcher, B., Koch, D., Kinne, S., Kondo, Y., Quinn, P.K., Sarofim, M.C., Schultz, M.G., Schulz, M., Venkataraman, C., Zhang, H., Zhang, S., Bellouin, N., Guttikunda, S.K., Hopke, P.K., Jacobson, M.Z., Kaiser, J.W., Klimont, Z., Lohmann, U., Schwarz, J.P., Shindell, D., Storelvmo, T., Warren, S.G., Zender, C.S., 2013. Bounding the role of black carbon in the climate system: A scientific assessment. J. Geophys. Res. - Atmos. 118, 5380-5552.

Bones, D.L., Henricksen, D.K., Mang, S.A., Gonsior, M., Bateman, A.P., Nguyen, T.B.,

25

533 Cooper, W.J., Nizkorodov, S.A., 2010. Appearance of strong absorbers and fluorophores in
534 limonene-O-3 secondary organic aerosol due to NH4+-mediated chemical aging over long
535 time scales. J. Geophys. Res. - Atmos. 115, D05203.

536 Bozzetti, C., Sosedova, Y., Xiao, M., Daellenbach, K.R., Ulevicius, V., Dudoitis, V.,
537 Mordas, G., Byčenkienė, S., Plauškaitė, K., Vlachou, A., Golly, B., Chazeau, B., Besombes,
538 J.-L., Baltensperger, U., Jaffrezo, J.-L., Slowik, J.G., El Haddad, I., Prévôt, A.S.H., 2017.
539 Argon offline-AMS source apportionment of organic aerosol over yearly cycles for an urban,
540 rural, and marine site in northern Europe. Atmos. Chem. Phys. 17, 117-141.

541 Budisulistiorini, S.H., Riva, M., Williams, M., Chen, J., Itoh, M., Surratt, J.D., Kuwata,
542 M., 2017. Light-absorbing brown carbon aerosol constituents from combustion of Indonesian
543 peat and biomass. Environ. Sci. Technol. 51, 4415-4423.

544 Canagaratna, M.R., Jimenez, J.L., Kroll, J.H., Chen, Q., Kessler, S.H., Massoli, P.,
545 Hildebrandt Ruiz, L., Fortner, E., Williams, L.R., Wilson, K.R., Surratt, J.D., Donahue, N.M.,
546 Jayne, J.T., Worsnop, D.R., 2015. Elemental ratio measurements of organic compounds using
547 aerosol mass spectrometry: characterization, improved calibration, and implications. Atmos.
548 Chem. Phys. 15, 253-272.

549 Cao, F., Zhang, S., Kawamura, K., Liu, X., Yang, C., Xu, Z., Fan, M., Zhang, W., Bao,
550 M., Chang, Y., Song, W., Liu, S., Lee, X., Li, J., Zhang, G., Zhang, Y., 2017. Chemical
551 characteristics of dicarboxylic acids and related organic compounds in PM2.5 during
552 biomass-burning and non-biomass-burning seasons at a rural site of Northeast China. Environ.
553 Pollut. 231, 654-662.

554 Cappa, C.D., Onasch, T.B., Massoli, P., Worsnop, D.R., Bates, T.S., Cross, E.S.,
555 Davidovits, P., Hakala, J., Hayden, K.L., Jobson, B.T., Kolesar, K.R., Lack, D.A., Lerner,
556 B.M., Li, S.-M., Mellon, D., Nuaaman, I., Olfert, J.S., Petäjä, T., Quinn, P.K., Song, C.,
557 Subramanian, R., Williams, E.J., Zaveri, R.A., 2012. Radiative Absorption Enhancements
558 Due to the Mixing State of Atmospheric Black Carbon. Science 337, 1078-1081.

559 Carslaw, K.S., Boucher, O., Spracklen, D.V., Mann, G.W., Rae, J.G.L., Woodward, S.,
560 Kulmala, M., 2010. A review of natural aerosol interactions and feedbacks within the Earth
561 system. Atmos. Chem. Phys. 10, 1701-1737.

562 Chakrabarty, R.K., Moosmuller, H., Chen, L.W.A., Lewis, K., Arnott, W.P., Mazzoleni,
563 C., Dubey, M.K., Wold, C.E., Hao, W.M., Kreidenweis, S.M., 2010. Brown carbon in tar balls
564 from smoldering biomass combustion. Atmos. Chem. Phys. 10, 6363-6370.

565 Chen, Q., Ikemori, F., Mochida, M., 2016. Light absorption and excitation-emission
566 fluorescence of urban organic aerosol components and their relationship to chemical structure.
567 Environ. Sci. Technol. 50, 10859-10868.

568 Chen, Q., Ikemori, F., Nakamura, Y., Vodicka, P., Kawamura, K., Mochida, M., 2017.
569 Structural and light-absorption characteristics of complex water-insoluble organic mixtures in
570 urban submicron aerosols. Environ. Sci. Technol. 51, 8293-8303.

571 Chen, Y., Bond, T.C., 2010. Light absorption by organic carbon from wood combustion.
572 Atmos. Chem. Phys. 10, 1773-1787.

573 Cheng, Y., Engling, G., He, K.B., Duan, F.K., Ma, Y.L., Du, Z.Y., Liu, J.M., Zheng, M.,
574 Weber, R.J., 2013. Biomass burning contribution to Beijing aerosol. Atmos. Chem. Phys. 13,
575 7765-7781.

576   Cheng, Y., He, K., Du, Z., Engling, G., Liu, J., Ma, Y., Zheng, M., Weber, R.J., 2016.
577   The characteristics of brown carbon aerosol during winter in Beijing. Atmos. Environ. 127,
578   355-364.

579   Cheng, Y., He, K., Zheng, M., Duan, F., Du, Z., Ma, Y., Tan, J., Yang, F., Liu, J., Zhang,
580   X., Weber, R., Bergin, M., Russell, A., 2011. Mass absorption efficiency of elemental carbon
581   and water-soluble organic carbon in Beijing, China. Atmos. Chem. Phys. 11, 11497-11510.

582   Chow, J.C., Watson, J.G., Lowenthal, D.H., Chen, L.W.A., Zielinska, B., Mazzoleni,
583   L.R., Magliano, K.L., 2007. Evaluation of organic markers for chemical mass balance source
584   apportionment at the Fresno Supersite. Atmos. Chem. Phys. 7, 1741-1754.

585   Daellenbach, K.R., Bozzetti, C., Křepelová, A., Canonaco, F., Wolf, R., Zotter, P.,
586   Fermo, P., Crippa, M., Slowik, J.G., Sosedova, Y., Zhang, Y., Huang, R.J., Poulain, L., Szidat,
587   S., Baltensperger, U., El Haddad, I., Prévôt, A.S.H., 2016. Characterization and source
588   apportionment of organic aerosol using offline aerosol mass spectrometry. Atmos. Meas. Tech.
589   9, 23-39.

590   Daellenbach, K.R., Stefenelli, G., Bozzetti, C., Vlachou, A., Fermo, P., Gonzalez, R.,
591   Piazzalunga, A., Colombi, C., Canonaco, F., Hueglin, C., 2017. Long-term chemical analysis
592   and organic aerosol source apportionment at 9 sites in Central Europe: Source identification
593   and uncertainty assessment. Atmos. Chem. Phys. 17, 13265-13282.

594   Desyaterik, Y., Sun, Y., Shen, X., Lee, T., Wang, X., Wang, T., Collett, J.L., 2013.
595   Speciation of "brown" carbon in cloud water impacted by agricultural biomass burning in
596   eastern China. J. Geophys. Res. - Atmos. 118, 7389-7399.

597   Du, Z., He, K., Cheng, Y., Duan, F., Ma, Y., Liu, J., Zhang, X., Zheng, M., Weber, R.,
598   2014. A yearlong study of water-soluble organic carbon in Beijing II: Light absorption
599   properties. Atmos. Environ. 89, 235-241.

600   Feng, Y., Ramanathan, V., Kotamarthi, V.R., 2013. Brown carbon: a significant
601   atmospheric absorber of solar radiation? Atmos. Chem. Phys. 13, 8607-8621.

602   Ge, X., Li, L., Chen, Y., Chen, H., Wu, D., Wang, J., Xie, X., Ge, S., Ye, Z., Xu, J.,
603   Chen, M., 2017. Aerosol characteristics and sources in Yangzhou, China resolved by offline
604   aerosol mass spectrometry and other techniques. Environ. Pollut. 225, 74-85.

605   Ge, X., Setyan, A., Sun, Y., Zhang, Q., 2012. Primary and secondary organic aerosols in
606   Fresno, California during wintertime: Results from high resolution aerosol mass spectrometry.
607   J. Geophys. Res. - Atmos. 117, D19301.

608   Ge, X., Shaw, S.L., Zhang, Q., 2014. Toward understanding amines and their
609   degradation products from postcombustion CO_2 capture processes with aerosol mass
610   spectrometry. Environ. Sci. Technol. 48, 5066-5075.

611   Ge, X., Wexler, A.S., Clegg, S.L., 2011a. Atmospheric amines - Part I. A review. Atmos.
612   Environ. 45, 524-546.

613   Ge, X., Wexler, A.S., Clegg, S.L., 2011b. Atmospheric amines - Part II.
614   Thermodynamic properties and gas/particle partitioning. Atmos. Environ. 45, 561-577.

615   Gyawali, M., Arnott, W.P., Lewis, K., Moosmüller, H., 2009. In situ aerosol optics in
616   Reno, NV, USA during and after the summer 2008 California wildfires and the influence of
617   absorbing and non-absorbing organic coatings on spectral light absorption. Atmos. Chem.
618   Phys. 9, 8007-8015.

619   Hecobian, A., Zhang, X., Zheng, M., Frank, N., Edgerton, E.S., Weber, R.J., 2010.
620   Water-soluble organic aerosol material and the light-absorption characteristics of aqueous
621   extracts measured over the Southeastern United States. Atmos. Chem. Phys. 10, 5965-5977.

622   Hems, R.F., Abbatt, J.P.D., 2018. Aqueous phase photo-oxidation of brown carbon
623   nitrophenols: Reaction kinetics, mechanism, and evolution of light absorption. ACS Earth
624   Space Chem. 2, 225-234.

625   Kim, H., Kim, J.Y., Jin, H.C., Lee, J.Y., Lee, S.P., 2016. Seasonal variations in the
626   light-absorbing properties of water-soluble and insoluble organic aerosols in Seoul, Korea.
627   Atmos. Environ. 129, 234-242.

628   Kirchstetter, T.W., Novakov, T., Hobbs, P.V., 2004. Evidence that the spectral
629   dependence of light absorption by aerosols is affected by organic carbon. J. Geophys. Res. -
630   Atmos. 109, D21208.

631   Kirillova, E.N., Andersson, A., Tiwari, S., Srivastava, A.K., Bisht, D.S., Gustafsson, Ö.,
632   2014. Water-soluble organic carbon aerosols during a full New Delhi winter: Isotope-based
633   source apportionment and optical properties. J. Geophys. Res. - Atmos. 119, 3476-3485.

634   Kirillova, E.N., Marinoni, A., Bonasoni, P., Vuillermoz, E., Facchini, M.C., Fuzzi, S.,
635   Decesari, S., 2016. Light absorption properties of brown carbon in the high Himalayas. J.
636   Geophys. Res. - Atmos. 121, 9621-9639.

637   Kroll, J.H., Donahue, N.M., Jimenez, J.L., Kessler, S.H., Canagaratna, M.R., Wilson,
638   K.R., Altieri, K.E., Mazzoleni, L.R., Wozniak, A.S., Bluhm, H., 2011. Carbon oxidation state
639   as a metric for describing the chemistry of atmospheric organic aerosol. Nat. Chem. 3, 133.

640   Lack, D.A., Langridge, J.M., Bahreini, R., Cappa, C.D., Middlebrook, A.M., Schwarz,
641   J.P., 2012a. Brown carbon and internal mixing in biomass burning particles. P. Natl. Aacd. Sci.
642   USA 109, 14802-14807.

643   Lack, D.A., Lovejoy, E.R., Baynard, T., Pettersson, A., Ravishankara, A.R., 2006.
644   Aerosol Absorption Measurement using Photoacoustic Spectroscopy: Sensitivity, Calibration,
645   and Uncertainty Developments. Aerosol Sci. Technol. 40, 697-708.

646   Lack, D.A., Richardson, M.S., Law, D., Langridge, J.M., Cappa, C.D., McLaughlin,
647   R.J., Murphy, D.M., 2012b. Aircraft Instrument for Comprehensive Characterization of
648   Aerosol Optical Properties, Part 2: Black and Brown Carbon Absorption and Absorption
649   Enhancement Measured with Photo Acoustic Spectroscopy. Aerosol Sci. Technol. 46,
650   555-568.

651   Laskin, A., Laskin, J., Nizkorodov, S.A., 2015. Chemistry of atmospheric brown carbon.
652   Chem. Rev. 115, 4335-4382.

653   Lee, H.J., Aiona, P.K., Laskin, A., Laskin, J., Nizkorodov, S.A., 2014. Effect of solar
654   radiation on the optical properties and molecular composition of laboratory proxies of
655   atmospheric brown carbon. Environ. Sci. Technol. 48, 10217-10226.

656   Lin, P., Aiona, P.K., Li, Y., Shiraiwa, M., Laskin, J., Nizkorodov, S.A., Laskin, A., 2016.
657   Molecular characterization of brown carbon in biomass burning aerosol particles. Environ.
658   Sci. Technol. 50, 11815-11824.

659   Lin, P., Liu, J., Shilling, J.E., Kathmann, S.M., Laskin, J., Laskin, A., 2015. Molecular
660   characterization of brown carbon (BrC) chromophores in secondary organic aerosol generated
661   from photo-oxidation of toluene. Physical chemistry chemical physics : PCCP 17,

28

662 23312-23325.

663 Liu, J., Bergin, M., Guo, H., King, L., Kotra, N., Edgerton, E., Weber, R.J., 2013.
664 Size-resolved measurements of brown carbon in water and methanol extracts and estimates of
665 their contribution to ambient fine-particle light absorption. Atmos. Chem. Phys. 13,
666 12389-12404.

667 Liu, J., Lin, P., Laskin, A., Laskin, J., Kathmann, S.M., Wise, M., Caylor, R., Imholt, F.,
668 Selimovic, V., Shilling, J.E., 2016. Optical properties and aging of light-absorbing secondary
669 organic aerosol. Atmos. Chem. Phys. 16, 12815-12827.

670 Liu, J., Scheuer, E., Dibb, J., Diskin, G.S., Ziemba, L.D., Thornhill, K.L., Anderson,
671 B.E., Wisthaler, A., Mikoviny, T., Devi, J.J., 2015. Brown carbon aerosol in the North
672 American continental troposphere: sources, abundance, and radiative forcing. Atmos. Chem.
673 Phys. 15, 5959-6007.

674 Mo, Y., Li, J., Liu, J., Zhong, G., Cheng, Z., Tian, C., Chen, Y., Zhang, G., 2017. The
675 influence of solvent and pH on determination of the light absorption properties of
676 water-soluble brown carbon. Atmos. Environ. 161, 90-98.

677 Nakayama, T., Ikeda, Y., Sawada, Y., Setoguchi, Y., Ogawa, S., Kawana, K., Mochida,
678 M., Ikemori, F., Matsumoto, K., Matsumi, Y., 2015. Properties of light‐absorbing aerosols in
679 the Nagoya urban area, Japan, in August 2011 and January 2012: Contributions of brown
680 carbon and lensing effect. J. Geophys. Res. - Atmos. 119, 12,721-712,739.

681 Nguyen, T.B., Lee, P.B., Updyke, K.M., Bones, D.L., Laskin, J., Laskin, A.,
682 Nizkorodov, S.A., 2012. Formation of nitrogen- and sulfur-containing light-absorbing
683 compounds accelerated by evaporation of water from secondary organic aerosols. J. Geophys.
684 Res. - Atmos. 117.

685 Petit, J.E., Favez, O., Albinet, A., Canonaco, F., 2017. A user-friendly tool for
686 comprehensive evaluation of the geographical origins of atmospheric pollution: Wind and
687 trajectory analyses. Environ. Modell. Softw. 88, 183-187.

688 Phillips, S.M., Bellcross, A.D., Smith, G.D., 2017. Light absorption by brown carbon in
689 the southeastern United States is pH-dependent. Environ. Sci. Technol. 51, 6782-6790.

690 Pokhrel, R.P., Beamesderfer, E.R., Wagner, N.L., Langridge, J.M., Lack, D.A.,
691 Jayarathne, T., Stone, E.A., Stockwell, C.E., Yokelson, R.J., Murphy, S.M., 2017. Relative
692 importance of black carbon, brown carbon, and absorption enhancement from clear coatings
693 in biomass burning emissions. Atmos. Chem. Phys. 17, 5063-5078.

694 Pokhrel, R.P., Wagner, N.L., Langridge, J.M., Lack, D.A., Jayarathne, T., Stone, E.A.,
695 Stockwell, C.E., Yokelson, R.J., Murphy, S.M., 2016. Parameterization of single-scattering
696 albedo (SSA) and absorption Ångström exponent (AAE) with EC / OC for aerosol emissions
697 from biomass burning. Atmos. Chem. Phys. 16, 9549-9561.

698 Polissar, A.V., Hopke, P.K., Paatero, P., Kaufmann, Y.J., Hall, D.K., Bodhaine, B.A.,
699 Dutton, E.G., Harris, J.M., 1999. The aerosol at Barrow, Alaska: long-term trends and source
700 locations. Atmos. Environ. 33, 2441-2458.

701 Saleh, R., Hennigan, C.J., McMeeking, G.R., Chuang, W.K., Robinson, E.S., Coe, H.,
702 Donahue, N.M., Robinson, A.L., 2013. Absorptivity of brown carbon in fresh and
703 photo-chemically aged biomass-burning emissions. Atmos. Chem. Phys. 13, 7683-7693.

704 Saleh, R., Robinson, E.S., Tkacik, D.S., Ahern, A.T., Liu, S., Aiken, A.C., Sullivan,

705   R.C., Presto, A.A., Dubey, M.K., Yokelson, R.J., Donahue, N.M., Robinson, A.L., 2014.
706   Brownness of organics in aerosols from biomass burning linked to their black carbon content.
707   Nat. Geosci. 7, 647.

708   Satish, R., Shamjad, P., Thamban, N., Tripathi, S., Rastogi, N., 2017. Temporal
709   characteristics of brown carbon over the central Indo-Gangetic plain. Environ. Sci. Technol.
710   51, 6765-6772.

711   Shamjad, P.M., Tripathi, S.N., Pathak, R., Hallquist, M., Arola, A., Bergin, M.H., 2015.
712   Contribution of brown barbon to direct radiative forcing over the Indo-Gangetic plain.
713   Environ. Sci. Technol. 49, 10474-10481.

714   Simoneit, B.R.T., 2002. Biomass burning — a review of organic tracers for smoke
715   from incomplete combustion. Appl. Geochem. 17, 129-162.

716   Simoneit, B.R.T., Schauer, J.J., Nolte, C.G., Oros, D.R., Elias, V.O., Fraser, M.P.,
717   Rogge, W.F., Cass, G.R., 1999. Levoglucosan, a tracer for cellulose in biomass burning and
718   atmospheric particles. Atmos. Environ. 33, 173-182.

719   Stein, A.F., Draxler, R.R., Rolph, G.D., Stunder, B.J.B., Cohen, M.D., Ngan, F., 2016.
720   NOAA's HYSPLIT atmospheric transport and dispersion modeling system. Bull. Am.
721   Meteorol. Soc. 96, 150504130527006.

722   Sumlin, B.J., Pandey, A., Walker, M.J., Pattison, R.S., Williams, B.J., Chakrabarty, R.K.,
723   2017. Atmospheric photooxidation diminishes light absorption by primary brown carbon
724   aerosol from biomass burning. Environ. Sci. Technol. Lett. 4, 540-545.

725   Teich, M., van Pinxteren, D., Wang, M., Kecorius, S., Wang, Z., Müller, T., Močnik, G.,
726   Herrmann, H., 2017. Contributions of nitrated aromatic compounds to the light absorption of
727   water-soluble and particulate brown carbon in different atmospheric environments in
728   Germany and China. Atmos. Chem. Phys. 17, 1653-1672.

729   Turpin, B.J., Huntzicker, J.J., 1995. Identification of secondary organic aerosol
730   episodes and quantitation of primary and secondary organic aerosol concentrations during
731   SCAQS. Atmos. Environ. 29, 3527-3544.

732   Updyke, K.M., Nguyen, T.B., Nizkorodov, S.A., 2012. Formation of brown carbon via
733   reactions of ammonia with secondary organic aerosols from biogenic and anthropogenic
734   precursors. Atmos. Environ. 63, 22-31.

735   Wang, G., Chen, C., Li, J., Zhou, B., Xie, M., Hu, S., Kawamura, K., Chen, Y., 2011.
736   Molecular composition and size distribution of sugars, sugar-alcohols and carboxylic acids in
737   airborne particles during a severe urban haze event caused by wheat straw burning. Atmos.
738   Environ. 45, 2473-2479.

739   Wang, G., Kawamura, K., Xie, M., Hu, S., Cao, J., An, Z., Waston, J.G., Chow, J.C.,
740   2009. Organic molecular compositions and size distributions of Chinese summer and autumn
741   aerosols from Nanjing: Characteristic haze event caused by wheat straw burning. Environ. Sci.
742   Technol. 43, 6493-6499.

743   Wang, G., Kawamura, K., Zhao, X., Li, Q., Dai, Z., Niu, H., 2007. Identification,
744   abundance and seasonal variation of anthropogenic organic aerosols from a mega-city in
745   China. Atmos. Environ. 41, 407-416.

746   Wang, J., Ge, X., Chen, Y., Shen, Y., Zhang, Q., Sun, Y., Xu, J., Ge, S., Yu, H., Chen,
747   M., 2016a. Highly time-resolved urban aerosol characteristics during springtime in Yangtze

748 River Delta, China: insights from soot particle aerosol mass spectrometry. Atmos. Chem.
749 Phys. 16, 9109-9127.

750 Wang, J., Nie, W., Cheng, Y., Shen, Y., Chi, X., Wang, J., Huang, X., Xie, Y., Sun, P.,
751 Xu, Z., Qi, X., Su, H., Ding, A., 2018. Light absorption of brown carbon in eastern China
752 based on 3-year multi-wavelength aerosol optical property observations at the SORPES
753 station and an improved Absorption Ångstrom exponent segregation method. Atmos. Chem.
754 Phys. Discuss., 1-31.

755 Wang, J., Onasch, T.B., Ge, X., Collier, S., Zhang, Q., Sun, Y., Yu, H., Chen, M.,
756 Prévôt, A.S., Worsnop, D.R., 2016b. Observation of fullerene soot in eastern China. Environ.
757 Sci. Technol. Lett. 3, 121-126.

758 Wang, J., Zhang, Q., Chen, M., Collier, S., Zhou, S., Ge, X., Xu, J., Shi, J., Xie, C., Hu,
759 J., Ge, S., Sun, Y., Coe, H., 2017. First chemical characterization of refractory black carbon
760 aerosols and associated coatings over the Tibetan plateau (4730 m a.s.l). Environ. Sci.
761 Technol. 51, 14072-14082.

762 Washenfelder, R.A., Attwood, A.R., Brock, C.A., Guo, H., Xu, L., Weber, R.J., Ng,
763 N.L., Allen, H.M., Ayres, B.R., Baumann, K., Cohen, R.C., Draper, D.C., Duffey, K.C.,
764 Edgerton, E., Fry, J.L., Hu, W.W., Jimenez, J.L., Palm, B.B., Romer, P., Stone, E.A.,
765 Wooldridge, P.J., Brown, S.S., 2015. Biomass burning dominates brown carbon absorption in
766 the rural southeastern United States. Geophys. Res. Lett. 42, 653-664.

767 Wu, C., Yu, J.Z., 2016. Determination of primary combustion source organic
768 carbon-to-elemental carbon (OC / EC) ratio using ambient OC and EC measurements:
769 secondary OC-EC correlation minimization method. Atmos. Chem. Phys. 16, 5453-5465.

770 Wu, D., Zhang, F., Ge, X., Yang, M., Xia, J., Liu, G., Li, F., 2017. Chemical and light
771 extinction characteristics of atmospheric aerosols in suburban Nanjing, China. Atmosphere 8,
772 149.

773 Xie, M., Chen, X., Hays, M.D., Lewandowski, M., Offenberg, J., Kleindienst, T.E.,
774 Holder, A.L., 2017. Light absorption of secondary organic aerosol: Composition and
775 contribution of nitroaromatic compounds. Environ. Sci. Technol. 51, 11607-11616.

776 Xu, J., Zhang, Q., Li, X., Ge, X., Xiao, C., Ren, J., Qin, D., 2013. Dissolved organic
777 matter and inorganic ions in a central Himalayan glacier—Insights into chemical composition
778 and atmospheric sources. Environ. Sci. Technol. 47, 6181-6188.

779 Xu, L., Guo, H., Weber, R.J., Ng, N.L., 2017. Chemical Characterization of
780 Water-Soluble Organic Aerosol in Contrasting Rural and Urban Environments in the
781 Southeastern United States. Environ. Sci. Technol. 51, 78-88.

782 Yan, C., Zheng, M., Bosch, C., Andersson, A., Desyaterik, Y., Sullivan, A.P., Collett,
783 J.L., Zhao, B., Wang, S., He, K., Gustafsson, O., 2017. Important fossil source contribution to
784 brown carbon in Beijing during winter. Scientific reports 7, 43182.

785 Yan, C., Zheng, M., Sullivan, A.P., Bosch, C., Desyaterik, Y., Andersson, A., Li, X.,
786 Guo, X., Zhou, T., Gustafsson, Ö., Collett, J.L., 2015. Chemical characteristics and
787 light-absorbing property of water-soluble organic carbon in Beijing: Biomass burning
788 contributions. Atmos. Environ. 121, 4-12.

789 Yang, M., Howell, S.G., Zhuang, J., Huebert, B.J., 2009. Attribution of aerosol light
790 absorption to black carbon, brown carbon, and dust in China – interpretations of

791 atmospheric measurements during EAST-AIRE. Atmos. Chem. Phys. 9, 2035-2050.

792 Ye, Z., Li, Q., Liu, J., Luo, S., Zhou, Q., Bi, C., Ma, S., Chen, Y., Chen, H., Li, L., Ge,
793 X., 2017a. Investigation of submicron aerosol characteristics in Changzhou, China:
794 Composition, source, and comparison with co-collected PM2.5. Chemosphere 183, 176-185.

795 Ye, Z., Li, Q., Ma, S., Zhou, Q., Gu, Y., Su, Y., Chen, Y., Chen, H., Wang, J., Ge, X.,
796 2017b. Summertime Day-Night Differences of PM2.5 Components (Inorganic Ions, OC, EC,
797 WSOC, WSON, HULIS, and PAHs) in Changzhou, China. Atmosphere 8, 189.

798 Ye, Z., Liu, J., Gu, A., Feng, F., Liu, Y., Bi, C., Xu, J., Li, L., Chen, H., Chen, Y., Dai,
799 L., Zhou, Q., Ge, X., 2017c. Chemical characterization of fine particulate matter in
800 Changzhou, China, and source apportionment with offline aerosol mass spectrometry. Atmos.
801 Chem. Phys. 17, 2573-2592.

802 Zhang, X., Lin, Y., Surratt, J.D., Weber, R.J., 2013. Sources, composition and
803 absorption Angstrom exponent of light-absorbing organic components in aerosol extracts
804 from the Los Angeles Basin. Environ. Sci. Technol. 47, 3685-3693.

805 Zhang, Y.-L., El-Haddad, I., Huang, R.-J., Ho, K.-F., Cao, J.-J., Han, Y., Zotter, P.,
806 Bozzetti, C., Daellenbach, K.R., Slowik, J.G., Salazar, G., Prévôt, A.S.H., Szidat, S., 2018.
807 Large contribution of fossil fuel derived secondary organic carbon to water soluble organic
808 aerosols in winter haze in China. Atmos. Chem. Phys. 18, 4005-4017.

809 Zhang, Y., Forrister, H., Liu, J., Dibb, J., Anderson, B., Schwarz, J.P., Perring, A.E.,
810 Jimenez, J.L., Campuzano-Jost, P., Wang, Y., Nenes, A., Weber, R.J., 2017a.
811 Top-of-atmosphere radiative forcing affected by brown carbon in the upper troposphere. Nat.
812 Geosci. 10, 486-489.

813 Zhang, Y., Tang, L., Sun, Y., Favez, O., Canonaco, F., Albinet, A., Couvidat, F., Liu, D.,
814 Jayne, J.T., Wang, Z., 2017b. Limited formation of isoprene epoxydiols‐derived secondary
815 organic aerosol under NOx‐rich environments in Eastern China. Geophys. Res. Lett. 44,
816 2035-2043.

817 Zhang, Y., Tang, L., Yu, H., Wang, Z., Sun, Y., Qin, W., Chen, W., Chen, C., Ding, A.,
818 Wu, J., 2015. Chemical composition, sources and evolution processes of aerosol at an urban
819 site in Yangtze River Delta, China during wintertime. Atmos. Environ. 123, 339-349.

820 Zhang, Y., Xu, J., Shi, J., Xie, C., Ge, X., Wang, J., Kang, S., Zhang, Q., 2017c. Light
821 absorption by water-soluble organic carbon in atmospheric fine particles in the central Tibetan
822 Plateau. Environ. Sci. Pollut. Res. 24, 21386-21397.

823 Zhao, R., Lee, A.K.Y., Huang, L., Li, X., Yang, F., Abbatt, J.P.D., 2015. Photochemical
824 processing of aqueous atmospheric brown carbon. Atmos. Chem. Phys. 15, 6087-6100.

825 Zhong, M., Jang, M., 2011. Light absorption coefficient measurement of SOA using a
826 UV‐Visible spectrometer connected with an integrating sphere. Atmos. Environ. 45,
827 4263-4271.

828 Zhu, C., Cao, J., Huang, R., Shen, Z., Wang, Q., Zhang, N., 2017. Light absorption
829 properties of brown carbon over the southeastern Tibetan Plateau. The Science of the total
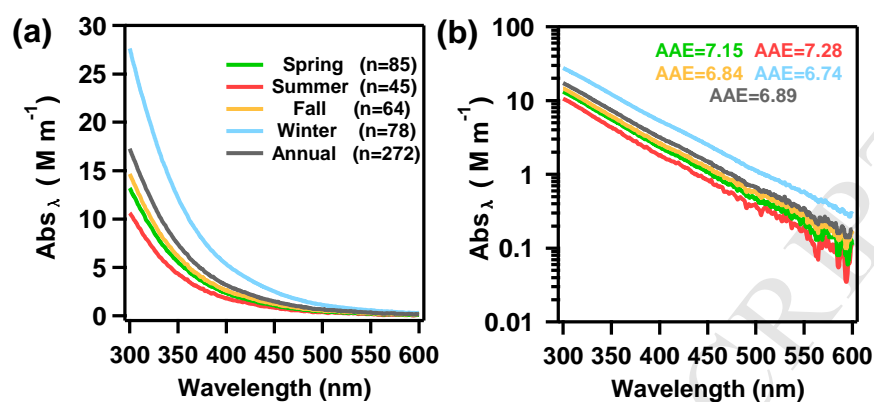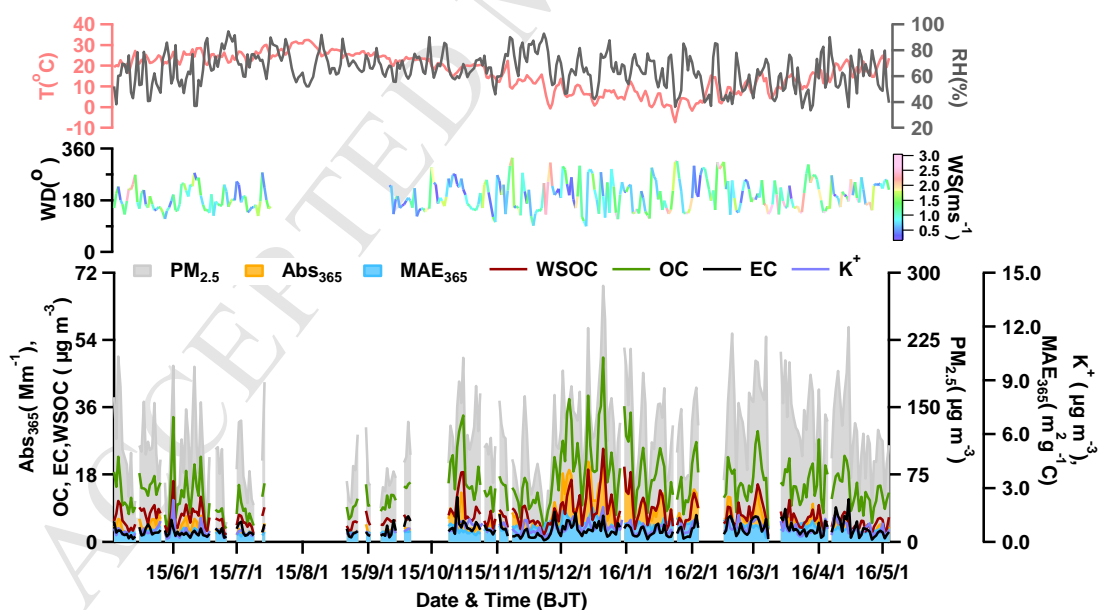830 environment 625, 246-251.

831

832

833

834 Figures

835

836 **Figure 1.** Seasonal and annual averaged light absorption spectra of water-soluble

837 aerosols: (a) linear scale and (b) log scale. The fitted Absorption Ångstrom Exponents
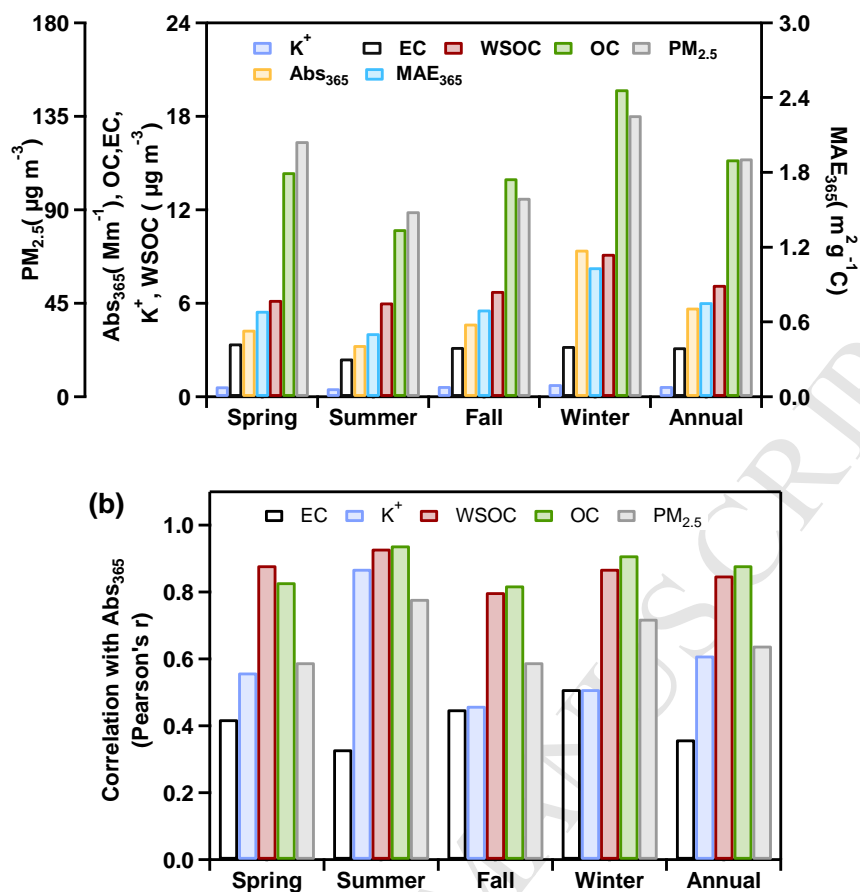
838 (AAE) are shown in (b).

839

840

841 **Figure 2.** Time series of (a) temperature (T) and relative humidity (RH), (b) wind

842 direction (WD) colored by wind speed (WS), (c) $PM_{2.5}$, WSOC, OC, K^+

843 concentrations, Abs365 and MAE_{365} during the study period (BJT, Beijing Time).

34

844

Figure 3. (a) Seasonal and annual averaged $PM_{2.5}$, WSOC, OC, K^+ concentrations,

Abs_{365} and MAE_{365}; (b) Correlation coefficients of Abs_{365} versus EC, K^+, WSOC, OC

and $PM_{2.5}$ during four seasons and the full year.

848

849
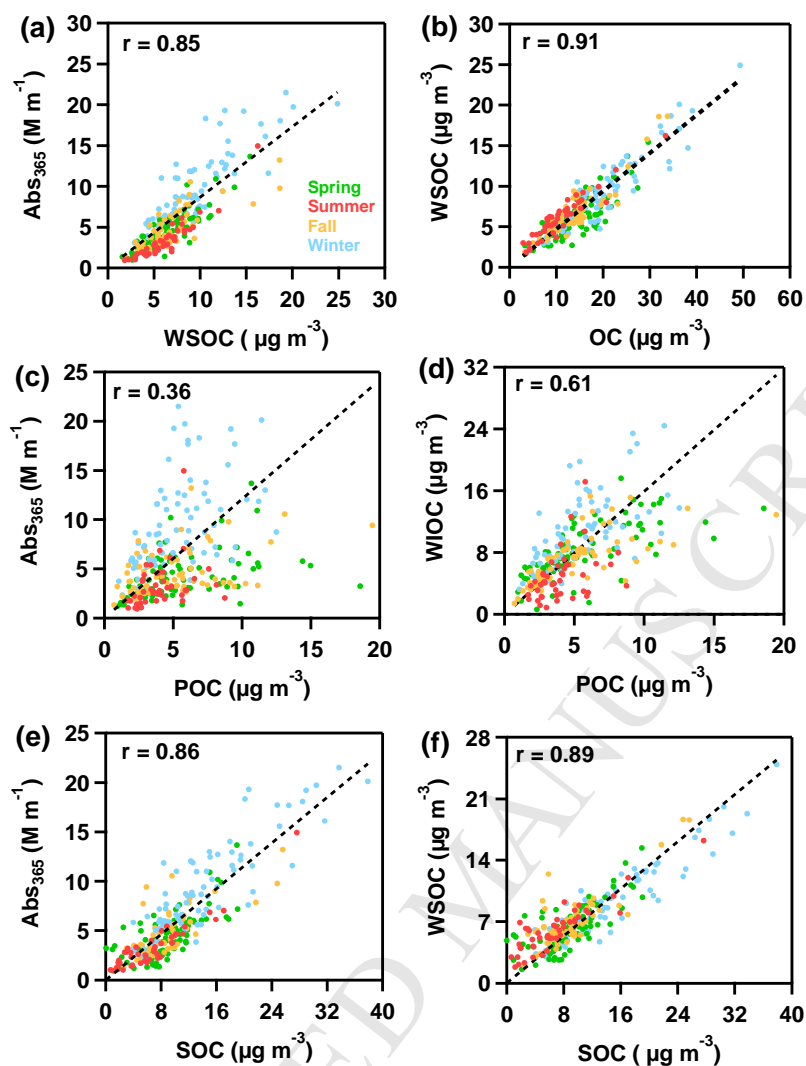
Figure 4. Scatter plots of (a) BrC Abs$_{365}$ versus water soluble organic carbon (WSOC),

(b) water-soluble organic carbon (WSOC) versus organic carbon (OC); (c) BrC Abs$_{365}$

versus primary organic carbon (POC), (d) water-insoluble organic carbon (WIOC)

versus primary organic carbon (POC), (e) BrC Abs$_{365}$ versus secondary organic carbon

(SOC), and (f) water-soluble organic carbon (WSOC) versus secondary organic

carbon (SOC) (data are classified into four seasons).

856

857
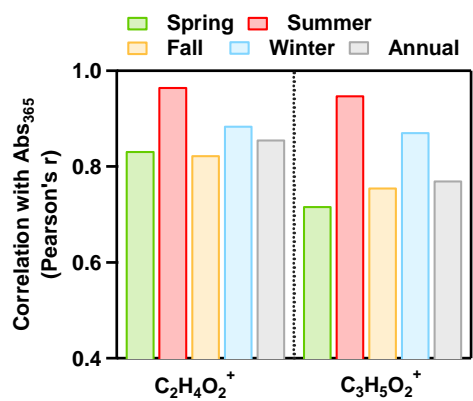
Figure 5. Correlation coefficients of Abs_{365} versus $C_2H_4O_2^+$ and $C_3H_5O_2^+$ for the four

seasons and full year.

860

861

862
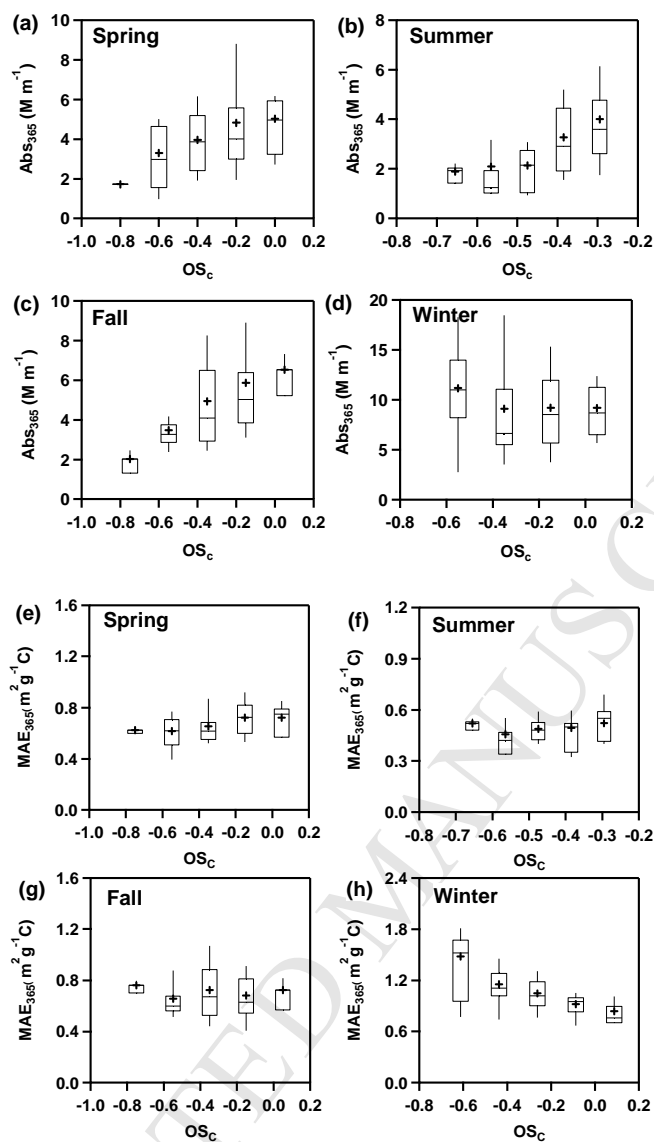
Figure 6. Abs_{365} and MAE_{365} as a function of OS_c during spring, summer, fall and winter (Data are grouped into a few bins. The whiskers above and below indicate the 90th and 10th percentiles, the upper and lower bounds of boxes represent the 75th and 25th percentiles, and the lines and crosses inside the boxes are median and mean values).
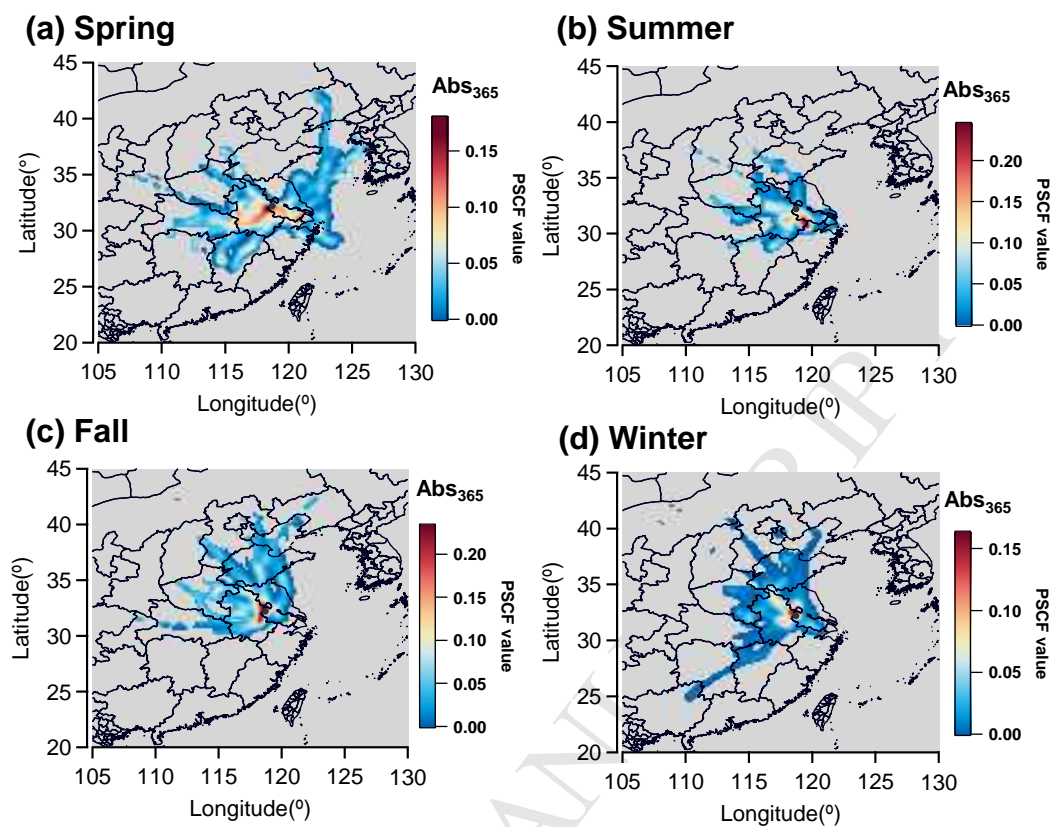
863

864

865

866

867

868

869

870
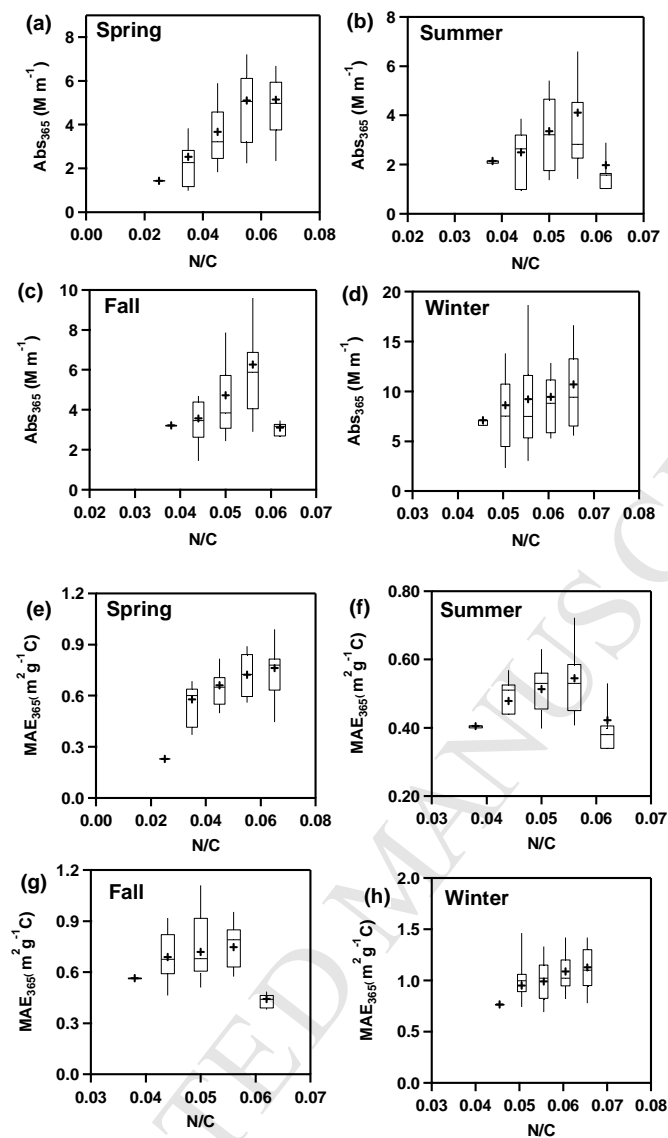
Figure 7. Abs$_{365}$ and MAE$_{365}$ as a function of N/C ratios during spring, summer, fall

and winter (Data are grouped into a few bins. Meanings of the boxes are the same as
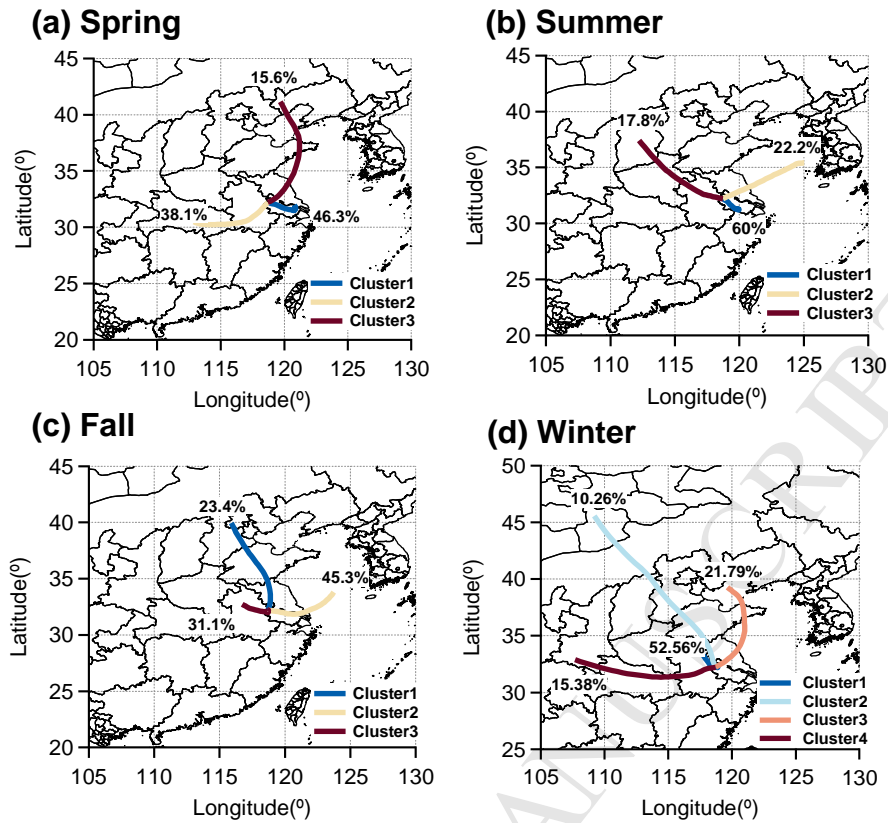
those described in Fig. 6).

39

875

Figure 8. The potential source contributions to BrC Abs$_{365}$ during (a) spring (b)

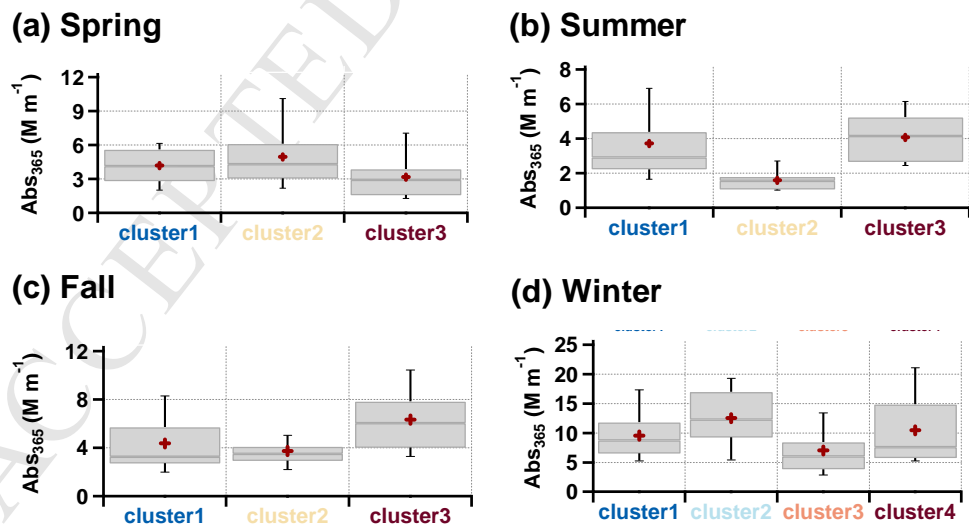summer (c) fall and (d) winter (colored by the PSCF values).

878

879

880 **Figure 9.** Clusters of the 36-h back trajectories during (a) spring (b) summer (c) fall

881 and (d) winter.

882

883 **Figure 10.** The average Abs_{365} values of the different clusters during (a) spring (b)

884 summer (c) fall and (d) winter.

41

Light absorption properties of one-year aerosol samples in Nanjing were characterized.

BrC light absorption is stronger during winter in Nanjing

BrC is closely associated with secondary organic species

BrC is influenced by biomass burning, especially in summer.

Nitrogen-containing organic compounds are likely BrC chromophores in Nanjing